


# Topological superconductors with spin-triplet pairings and Majorana Fermi arcs

Shi Huang(黄石) and Xi Luo(罗熙)

**Citation:**Chin. Phys. B, 2024, 33 (**8**): 087301. DOI: 10.1088/1674-1056/ad462f

**What follows is a list of articles you may be interested in**

---

## Chiral symmetry protected topological nodal superconducting phase and Majorana Fermi arc

Mei-Ling Lu(卢美玲), Yao Wang(王瑶), He-Zhi Zhang(张鹤之), Hao-Lin Chen(陈昊林), Tian-Yuan Cui(崔天元), and Xi Luo(罗熙)
Chin. Phys. B, 2023, 32 (**2**): 027301. DOI: 10.1088/1674-1056/ac7208

## Magneto-transport properties of thin flakes of Weyl semiconductor tellurium

Nan Zhang(张南), Bin Cheng(程斌), Hui Li(李惠), Lin Li(李林), and Chang-Gan Zeng(曾长淦)
Chin. Phys. B, 2021, 30 (**8**): 087304. DOI: 10.1088/1674-1056/ac0a5e

## Surface states modulated exchange interaction in $Bi_2Se_3$/thulium iron garnet heterostructures

Hai-Bin Shi(石海滨), Li-Qin Yan(闫丽琴), Yang-Tao Su(苏仰涛), Li Wang(王力), Xin-Yu Cao(曹昕宇), Lin-Zhu Bi(毕林竹), Yang Meng(孟洋), Yang Sun(孙阳), and Hong-Wu Zhao(赵宏武)
Chin. Phys. B, 2020, 29 (**11**): 117302. DOI: 10.1088/1674-1056/abbbdf

## Electrical spin polarization through spin-momentum locking in topological-insulator nanostructures

Minhao Zhang(张敏昊), Xuefeng Wang(王学锋), Fengqi Song(宋凤麒), Rong Zhang(张荣)
Chin. Phys. B, 2018, 27 (**9**): 097307. DOI: 10.1088/1674-1056/27/9/097307

## Elastic scattering of surface states on three-dimensional topological insulators

Wang Jing (王靖), Zhu Bang-Fen (朱邦芬)
Chin. Phys. B, 2013, 22 (**6**): 067301. DOI: 10.1088/1674-1056/22/6/067301

---

# Topological superconductors with spin-triplet pairings and Majorana Fermi arcs

Shi Huang(黄石) and Xi Luo(罗熙)†

*College of Science, University of Shanghai for Science and Technology, Shanghai* 200093, *China*

(Received 11 January 2024; revised manuscript received 19 April 2024; accepted manuscript online 2 May 2024)

We construct a three-dimensional topological superconductor Bogoliubov–de Gennes (BdG) Hamiltonian with the normal state being a three-dimensional topological insulator. By introducing inter-orbital spin-triplet pairings term $\Delta_3$, there are topological Majorana nodes in the bulk and they are connected by Majorana Fermi arcs on the surface, similar to the case of Weyl semimetal. Furthermore, by adding an inversion-breaking term to the normal state, momentum-independent pairing terms with different parities can coexist in the BdG Hamiltonian, which creates more Majorana modes similar to Andreev bound states and a richer phase diagram.

**Keywords:** topological surface states, topological superconductors, topological nodes, Weyl points, Majorana Fermi arcs

**PACS:** 73.20.At, 74.20.–z, 03.65.Vf **DOI:** 10.1088/1674-1056/ad462f

## 1. Introduction

In the last decade, the understanding of topological structures without gaps has developed significantly. One famous example is Weyl semimetals. These are three-dimensional examples of nontrivial gapless band structures, where Weyl points protected by nontrivial winding numbers can be considered as "monopoles" of the Berry phase.[1–7] According to the bulk–edge correspondence, chiral Weyl points are connected by Fermi arcs and these are related to the two-dimensional Chern numbers. By choosing a momentum along the Fermi arc direction, when the Chern number corresponding to the bulk state is nonzero, the system's Hamiltonian can be simplified to a gapless quasi-two-dimensional system between edge states and the gapless edge states corresponding to Fermi arcs. In other words, Weyl semimetals are intermediate states between topological insulators and ordinary insulators.[3,7,8] In addition to Weyl semimetals, topological semimetals also include Dirac semimetals,[7,9] nodal line semimetals.[10,11] and multi-point semimetals.[12,13] Beyond condensed matter physics, the concept of topological states has gradually been applied in other classical physics fields, such as topological Weyl magnets,[14] topological phonons,[15–17] topological photonics and topological non-Hermitian systems.[18–20] Additionally, due to the potential applications of Majorana zero modes in topological superconductors in quantum computing, topological superconductors have attracted considerable attention.[21–24] The bulk state of a topological superconductor has a topological energy gap, while the surface hosts zero-energy modes composed of Majorana Fermions.[25] In 2001, Kitaev proposed a one-dimensional topological superconducting model where Majorana zero modes exist at the ends of the model.[22] In 2008, Fu and Kane studied the quasiparticle behavior of stable individual Majorana zero modes in the non-degenerate superconducting Dirac surface states of a two-dimensional superconductor, demonstrating that stable single Majorana zero modes can exist in the superconducting magnetic flux vortices at the interface between an s-wave superconductor and a topological insulator.[26] After the discovery of topological insulator materials, it was found that doping of these materials may induce superconducting states, such as $Cu_xBi_2Se_3$, $Sr_xBi_2Se_3$ and $Tl_xBi_2Te_3$.[27] Since the discovery of topological superconductors, research on topological nodes and Majorana arcs has increased significantly. For instance, the stability of line node superconductor structures in high-$T_c$ materials and mixed singlet-triplet superconducting states have been examined.[28] Breaking inversion symmetry may lead to the opening of gaps at Dirac nodes, forming three-dimensional Dirac superconductors.[29] Majorana fermions have also been shown to exist in nodal superconductors under conditions induced by antisymmetric spin-orbit interaction and a nonzero magnetic field below the upper critical field.[30] Recently, an iron-based superconducting phase was found in these materials FeTeSe,[31–34] whose normal state is a topological insulator. These results motivated us to study the possible pairings in such systems with the normal state being a topological insulator.

In this paper we construct a three-dimensional superconductor model based on a topological insulator. We consider the possible momentum-independent pairings and discuss their band structures and surface states. By introducing an inter-orbital spin triplet pairing there will be topological protected

†Corresponding author. E-mail: xiluo@usst.edu.cn

© 2024 Chinese Physical Society and IOP Publishing Ltd 

Majorana nodes and they are connected by Majorana Fermi arcs when an open boundary condition is applied, which is a superconducting analog of a Weyl semimetal.[3,7,8] This paper is organized as follows. In Section 2, we start from the Bernevig–Hughes–Zhang (BHZ) model that describes the normal state of a topological insulator, then we add the inter-orbital spin triplet term and there are topologically protected Majorana nodes and Majornan Fermi arcs in the system. In Section 3, by breaking inversion symmetry, different parities of superconducting pairings can coexist, we find that more Majorana nodes emerge and discuss the phase diagram and band structure in this situation. Section 4 is devoted to conclusions, and we provide the band structures with the same parity of two different pairings in Appendix A.

## 2. Model Hamiltonian

### 2.1. Three-dimensional topological insulator

The Hamiltonian form of the three-dimensional BHZ model[35] is

$$h_0^{3\mathrm{D}}(\boldsymbol{q}) = v(\sin(q_i)\sigma_i\rho_x) + \boldsymbol{M}(\boldsymbol{q})\sigma_0\rho_z - \mu\sigma_0\rho_0, \tag{1}$$

where $M(\boldsymbol{q}) = M_0 - M_1(\cos(q_x)+\cos(q_y)) - M_2\cos(q_z)$, $\sigma_i$, $\rho_i$ are Pauli matrices acting on spin and orbital degrees of freedom. The orbital degree of freedom originates from orbital hybridization; for example, there is a spin–orbit coupled p-orbital in HgTe or hybridization between the 6p orbitals of Bi and the 4p orbitals of Te in $Bi_2Te_3$.[35,36] In addition, $\upsilon$ is a hopping parameter, set to 1 in this study, and $\mu$ is chemical potential. Different numerical values of $M_i$ will result in different phases. The band inversion at $Z$ point occurs when $M_0 < 0$, $M_1 < 0$, $M_2 > 0$, $2M_1 - M_2 < M_0 < \min\{-M_2, -|2M_1 + M_2|\}$.[37] Choosing $M_0 = -8.5$, $M_1 = -3$, $M_2 = 3$ satisfies the above parameter range. It is a topological insulator (see Fig. 1), the band inversion occurs at the $Z$ point and it has topological surface states with Dirac cone-type dispersion when open boundary condition is supplied. The BHZ model Hamiltonian has TRS, i.e., $\boldsymbol{T}h_0(\boldsymbol{q})\boldsymbol{T}^{-1} = h_0(-\boldsymbol{q})$. Here, $\boldsymbol{T} = \mathrm{i}\sigma_y\rho_0\kappa$ is the time-reversal operator and $\kappa$ represents the complex conjugate operator. In TRS systems, energy levels exhibit Krammers degeneracy, with each band corresponding to an even number of eigenstates. Similarly, inversion symmetry can be defined as $\boldsymbol{P}h_0^{3\mathrm{D}}(\boldsymbol{q})\boldsymbol{P}^{-1} = h_0^{3\mathrm{D}}(-\boldsymbol{q})$, where $\boldsymbol{P} = \sigma_0\rho_z$ is the inversion operator.

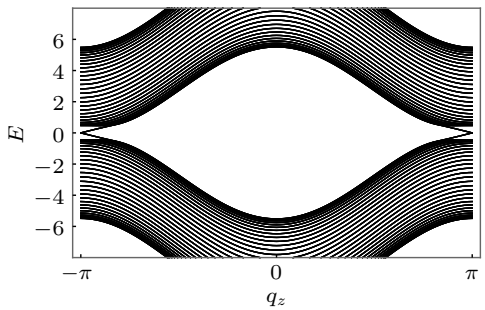



**Fig. 1.** Band structures of a topological insulator, $q_x = 0$, $y = 30$, $\mu = 0$, $M_0 = -8.5$, $M_1 = -3$, $M_2 = 3$.

### 2.2. Three-dimensional topological superconductor with spin-triplet pairing and Majorana Fermi arcs

We have chosen the Nambu basis as

$$\begin{aligned}\Psi_N = \big\{&\psi_{1\uparrow\boldsymbol{q}}, \psi_{1\downarrow\boldsymbol{q}}, \psi_{2\uparrow\boldsymbol{q}}, \psi_{2\downarrow\boldsymbol{q}},\\ &\psi^\dagger_{1\uparrow-\boldsymbol{q}}, \psi^\dagger_{1\downarrow-\boldsymbol{q}}, \psi^\dagger_{2\uparrow-\boldsymbol{q}}, \psi^\dagger_{2\downarrow-\boldsymbol{q}}\big\}^{\mathrm{T}},\end{aligned} \tag{2}$$

where $\boldsymbol{q}$ represents momentum, $\uparrow\downarrow$ denotes spin direction, and 1 and 2 label different orbits. This can arise from orbital hybridization, e.g., $FeSe_{0.5}Te_{0.5}$, there is orbital hybridization between orbitals $d_{xy}$ and $p_z$,[38] due to the band inversion between the orbits, the normal state is a topological insulator. There are six kinds of possible nonvanishing momentum-independent s-wave pairing terms in our model. Therefore, on the Nambu basis of Eq. (3), introducing the inter-orbital spin triplet $\Delta_3$ term firstly (for more possible pairings see Section 3).[39] We construct the topological superconductor BdG Hamiltonian as follows:

$$H_{\mathrm{BdG}}(\boldsymbol{q}) = \begin{pmatrix} h_0^{3\mathrm{D}}(\boldsymbol{q}) & \Delta_3^\dagger \\ \Delta_3 & -h_0^{3\mathrm{D}*}(-\boldsymbol{q}) \end{pmatrix}, \tag{3}$$

where $\Delta_3 = \delta_3 \cdot \mathrm{i}\sigma_x\rho_y$, $\delta_3$ is a constant, being superconducting pairing strength, and $\Delta_3$ breaks the TRS of the normal state. Such a BdG Hamiltonian may exist in iron-based superconductors.[40–42] For example, in Ref. [39], in a two-layer system, these pairing terms can be induced from electron–electron interactions. The microscopic mechanism for inducing the pairing terms from the electron interaction is beyond the scope of this paper and will be studied in future works.

The BCS superconducting theory proposes the introduction of superconducting pairing under the mean-field approximation. Therefore, in superconducting systems, the creation and annihilation operators always appear in pairs. The BdG Hamiltonian is obtained based on the Nambu basis, where the first half of the Nambu basis consists of annihilation operators for electrons and the second half consists of creation operators for electrons. Due to the relationship between electrons and holes, it naturally possesses an additional symmetry known as particle–hole symmetry (PHS).[43–45] The PHS operator $\boldsymbol{C} = \sigma_0\rho_0\tau_x\kappa$. The specific form of PHS is given by

$$\boldsymbol{C}H_{\mathrm{BdG}}(\boldsymbol{q})\boldsymbol{C}^{-1} = -H_{\mathrm{BdG}}(-\boldsymbol{q}). \tag{4}$$

The effect of PHS on the band structure is manifested in the symmetry of the bands about the Fermi surface. In other words, a Hamiltonian with PHS is always centrosymmetric above and below the Fermi surface.

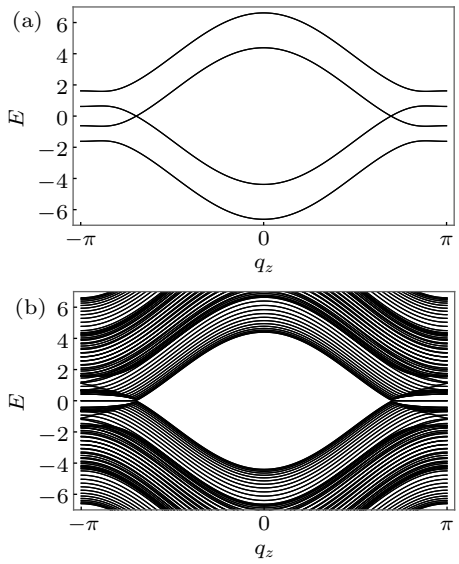



**Fig. 2.** Periodic and open boundary BdG Hamiltonian band structures $M_0 = -8.5$, $M_1 = -3$, $M_2 = 3$, $q_x = 0$, $q_y = 0$, $\mu = 1$, $\delta_{1,2,4,5,6} = 0$, $\delta_3 = 1$, (a) periodic boundary band structure, (b) open boundary (along $y$-direction, $y = 30$) band structure.

In Fig. 2, as the inter-orbital spin triplet strength $\delta_3$ increases from 0, two bands approach each other, leading to a change in the number of Weyl points from 2 before returning to 0. The pair of Weyl points move inward along the $q_z$-direction and eventually coincide at the $\Gamma$ point, resulting in the opening of the gap. At the same time, in the case of open boundaries, the Marjoram Fermi arc appears when the Weyl points first emerge. These Majorana Fermi arcs and Majorana nodes are topologically protected. Away from the nodal point, with the value of $q_z$ fixed, the Hamiltonian takes on a quasi-two-dimensional form, $H(q_x, q_y, q_{z0})$, then we can define the Chern number of the system. The Chern number can be calculated numerically using

$$\begin{aligned} \boldsymbol{n} = \frac{\mathrm{i}}{8\pi^2}\int \mathrm{d}^2\boldsymbol{q}\,\mathrm{d}\omega\,\mathrm{Tr}[G^2(\partial_{q_y}H)G(\partial_{q_x}H) \\ - G^2(\partial_{q_x}H)G(\partial_{q_y}H)], \end{aligned} \tag{5}$$

where $G = (H - \mathrm{i}\omega)^{-1}$ and $\boldsymbol{q} = (q_x, q_y)$.[46] For example, in Fig. 2, if the Majorana Fermi arc exists, then the corresponding quasi-2D Chern number is 1, and if the Majorana Fermi arc does not exist, then the Chern number is 0. The zero energy states of the Majorana edge modes correspond to the Majorana Fermi arcs. The case here is similar to that of a Fermi arc in Weyl semimetal. These Majorana Fermi arcs resemble Andreev bound states such that the two cases may not be distinguishable within experimental resolution.[47] The Majorana Fermi arcs may lead to pronounced anomalies at low energies in the scanning tunneling spectra and differential conductance $\mathrm{d}I/\mathrm{d}V$ and behave differently from the metal state. A detailed study of the $\mathrm{d}I/\mathrm{d}V$ behavior of the Majorana arc states will be conducted in future works.[47–49]

## 3. Inversion-breaking topological phase diagram and energy spectrum

In the former section, we considered a topological insulator with inversion symmetry, here we consider the inversion breaking. When inversion is broken, pairing terms with different parities can coexist. Besides the inter-orbital spin triplet term $\Delta_3$, there are other non-vanishing superconducting pairing terms $\Delta_1$, $\Delta_2$, $\Delta_4$, $\Delta_5$, $\Delta_6$ representing inter(intra)-orbital spin singlet (triplet) terms. To be precise, $\Delta_1 = \mathrm{i}\sigma_y\rho_x$, $\Delta_2 = \mathrm{i}\sigma_y\rho_z$, $\Delta_4 = \mathrm{i}\sigma_y\rho_0$, $\Delta_5 = \mathrm{i}\sigma_0\rho_y$, $\Delta_6 = \mathrm{i}\sigma_z\rho_y$.[39] Setting constants $\delta_i$ as superconducting pairing $\Delta_i$ strength, respectively, and verifying the TRS and inversion symmetry parity of $\Delta_i$

$$\boldsymbol{T}\Delta_{1,2,4,5}\boldsymbol{T}^{-1} = \Delta_{1,2,4,5}, \tag{6}$$

$$\boldsymbol{T}\Delta_{3,6}\boldsymbol{T}^{-1} = -\Delta_{3,6}, \tag{7}$$

and

$$\boldsymbol{P}\Delta_{1,3,5,6}\boldsymbol{P}^{-1} = -\Delta_{1,3,5,6}, \tag{8}$$

$$\boldsymbol{P}\Delta_{2,4}\boldsymbol{P}^{-1} = \Delta_{2,4}, \tag{9}$$

which means when $\Delta_3$, $\Delta_6$ is non-zero, TRS is broken. In addition $\Delta_1$, $\Delta_3$, $\Delta_5$, $\Delta_6$ are inversion-odd and $\Delta_2$, $\Delta_4$ are inversion-even. Due to the presence of the inversion symmetry, all six pairing terms with different inversion parity could not coexist. Therefore, for all six kinds of pair terms to coexist, inversion symmetry must be broken, which can be achieved by adding a term that breaks inversion symmetry in the normal states.

$$h_0^{\mathrm{IB}}(\boldsymbol{q}) = h_0^{\mathrm{3D}}(\boldsymbol{q}) + u\sigma_0\rho_x, \tag{10}$$

$$H_{\mathrm{BdG}}^{\mathrm{IB}}(\boldsymbol{q}) = H_{\mathrm{BdG}}(\boldsymbol{q}) + u\sigma_0\rho_x\tau_z, \tag{11}$$

where the $u$ term breaks inversion symmetry, in the subsequent section, $u$ is set to 1. Figure 3 (figure 4) illustrates band structures with nonzero superconducting pairing terms under periodic (open) boundary condition. Checking the BDG Hamiltonian with every single pairing term one by one, we can find that with some specific values of $\Delta_2$, $\Delta_3$, $\Delta_4$ or $\Delta_6$, edge states can be observed (see Figs. 4(b)–4(d) and 4(f)). They are fully gapped topological superconducting states. According to the ten-fold classification, the system belongs to DIII, and this is classified by $\mathbb{Z}$ in three dimensions when TRS is protected.[50] Although $\Delta_3$ and $\Delta_6$ break the original TRS, a new TRS operator can be found with $\boldsymbol{T}' = \mathrm{i}\sigma_y\rho_0\tau_z\kappa$. If only pairing terms $\delta_1$ or $\delta_5$ were nonzero, they correspond to trivial topological states (see Figs. 4(a) and 4(e)).

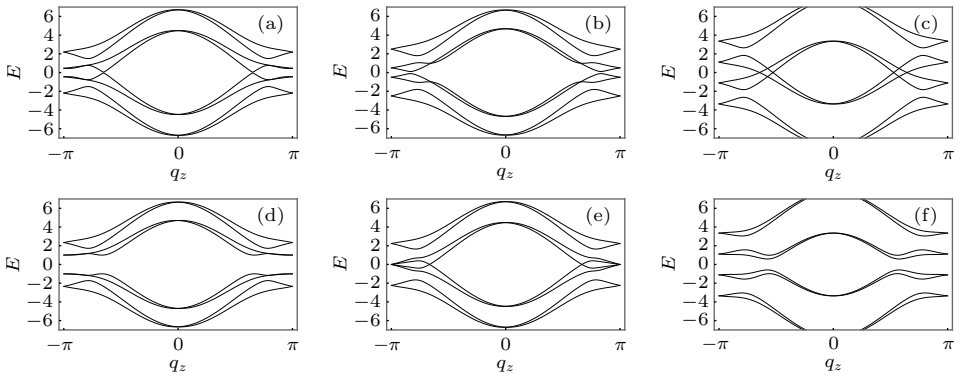



**Fig. 3.** BdG Hamiltonian band structure with different single superconducting pairing and inversion-breaking term. $M_0 = -8.5$, $M_1 = -3$, $M_2 = 3$, $q_x = 0$, $q_y = 0$, $\mu = 1$, $u = 1$: (a) $\delta_1 = 0.5$, (b) $\delta_2 = 1$, (c) $\delta_3 = 2$, (d) $\delta_4 = 1$, (e) $\delta_5 = 0.5$, (f) $\delta_6 = 2$.

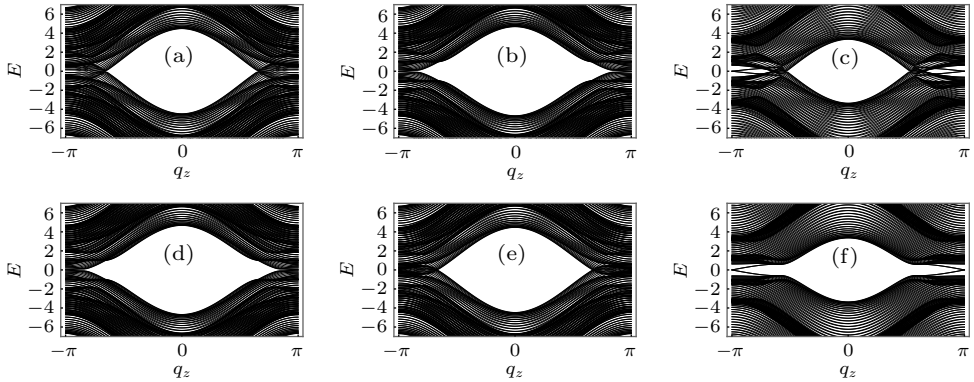



**Fig. 4.** Open boundary condition band structure with different single superconducting pairing and inversion breaking term. $M_0 = -8.5$, $M_1 = -3$, $M_2 = 3$, $q_x = 0$, $q_y = 0$, $\mu = 1$, $u = 1$: (a) $\delta_1 = 0.5$, (b) $\delta_2 = 1$, (c) $\delta_3 = 2$, (d) $\delta_4 = 1$, (e) $\delta_5 = 0.5$, (f) $\delta_6 = 2$.

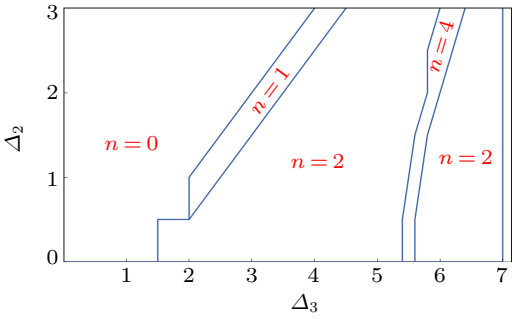



**Fig. 5.** Topological phase diagrams of $H_{\mathrm{BdG}}^{\mathrm{IB}}$ in $\Delta_2$–$\Delta_3$ plane with $M_0 = -8.5$, $M_1 = -3$, $M_2 = 3$, $q_x = 0$, $q_y = 0$, $\mu = 1$, $u = 1$, $\delta_{1,4,5,6} = 0$, we choose an open boundary condition along the $y$-direction and manually check the number of edge states which are presented by $n$.

Without loss of generality, we consider two pairing terms with different parities, for example $\Delta_2$ and $\Delta_3$, and we consider the phase diagram. Utilizing Eq. (10), we compute the eigenspectrum of the Hamiltonian, which depends on the values of $\Delta_2$ and $\Delta_3$. Due to the complexity of the band structure and the potential errors introduced by computational precision, accurately solving for the boundaries of the topological phase is a challenging task. As a result, we discretize the parameter space as running from 0 to 7 for $\Delta_3$ and 0 to 3 for $\Delta_2$ with the step being 0.2 and 0.5. We draw the band structures with open and periodic boundary conditions and manually check the topological phases. The resulting phase diagram is depicted in Fig. 5, where $n$ represents the number of the pairing edge states. We choose some specific points $\delta_2 = 0.5, \delta_3 = 2$ and $\delta_2 = 1, \delta_3 = 6$, and plot the band structure with open (periodic) boundary conditions (see Fig. 6). The presence of nonzero values for both $\Delta_2$ and $\Delta_3$ leads to the complete breaking of the inversion symmetry in the BdG Hamiltonian. This results in an asymmetry within the band structure, causing Majorana Fermi arcs to reconstruct. As the value of $\delta_3$ gradually increases, the topological nodes and edge states will gradually move from the $Z$ points towards the $\Gamma$ point. Comparing Fig. 6(d) to Fig. 6(b), the topological nodes and the Majorana points do not exhibit a one-to-one correspondence because the phase diagram under periodic boundary conditions is only plotted along the $q_y = 0$ direction, failing to depict nodes when $q_y \neq 0$. In Fig. 7, we show that there are Majorana points emerging for $q_y \neq 0$. Due to computational limitations, we choose an energy cutoff $E = 0.2$ to find the Majorana points that correspond to the Fermi pocket structures in Fig. 7. Region $n = 4$ of Fig. 5 implies that the topological nodes emerging with $q_y \neq 0$ and the nodes present in the periodic boundary condition band structure both appear in the first Brillouin zone, causing four pairs of Majorana Fermi arcs. As $\delta_3$ increases, the topological nodes in the band structure under periodic boundary conditions meet at the $\Gamma$ point and a gap opens, resulting in a reduction in the number of edge states. This process corresponds to the transition from $n = 4$ to $n = 2$, as depicted in

Fig. 5.

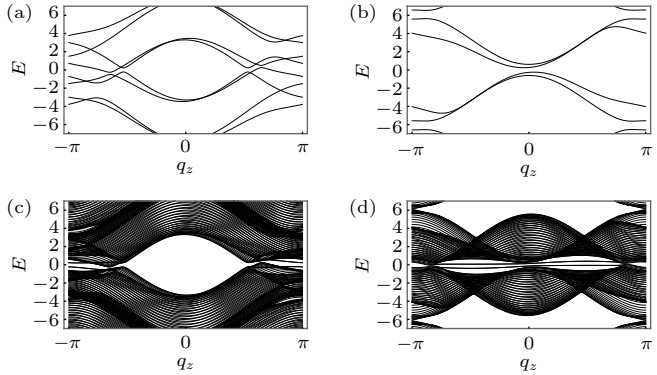



**Fig. 6.** Periodic and open boundary (along $y$-direction, $y = 30$) BdG Hamiltonian band structures. $M_0 = -8.5$, $M_1 = -3$, $M_2 = 3$, $q_x = 0$, $q_y = 0$ $\mu = 1$, $u = 1$, $\delta_{1,4,5,6} = 0$: (a), (c) $\delta_2 = 0.5$, $\delta_3 = 2$, (b), (d) $\delta_2 = 1$, $\delta_3 = 6$.

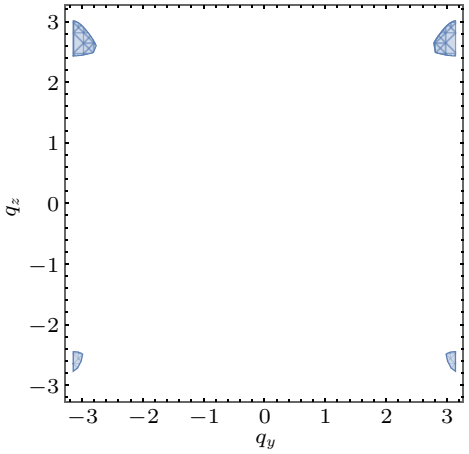



**Fig. 7.** The shadow parts are the fermi pockets near the Majorana points with energy $|E| \leqslant 0.2$. Range of $q_y$ and $q_z$ values when additional Majorana points are present with $M_0 = -8.5$, $M_1 = -3$, $M_2 = 3$, $q_x = 0$, $\mu = 1$, $u = 1$, $\delta_{1,4,5,6} = 0$, $\delta_2 = 1, \delta_3 = 6$.

In Appendix A, we consider the effects of pairings with the same parity, for example $\delta_1$ and $\delta_3$. We find similar behavior of the Majorana Fermi arcs, due to the inversion breaking of the normal state.

## 4. Conclusion

In summary, we study the topological properties of a topological superconductor with momentum independent pairings with the normal state being a topological insulator. When the inter-orbital spin triplet pairing term is nonzero, the TRS is broken, Majorana points emerge and the Majorana Fermi arcs connect them under an open boundary condition. Considering other non-vanishing superconducting pairing terms, due to the different parity of these terms, we break inversion symmetry to allow them to coexist. There are more Majorana points and topological phases with the coexistence of superconducting pairing terms.

## Appendix A: More band structures in the phase diagram

We also discussed the situation where pairing terms with the same inversion symmetry simultaneously exist, such as $\Delta_1$ and $\Delta_3$. When $\delta_1$ and $\delta_3$ are within some ranges, Marjorana nodes and Marjorana Fermi arcs will also appear. The band structures of the periodic and open boundary BdG Hamiltonian with varying $\Delta_1$ and $\Delta_3$ are illustrated in Fig. A1. Compared to altering $\Delta_2$ and $\Delta_3$, changing $\Delta_1$ and $\Delta_3$ introduces more edge state behaviors. Thus, by adjusting different superconducting pairing terms, we can modify the behaviors of topological nodes and Majorana Fermi arcs to achieve the desired structural outcome.

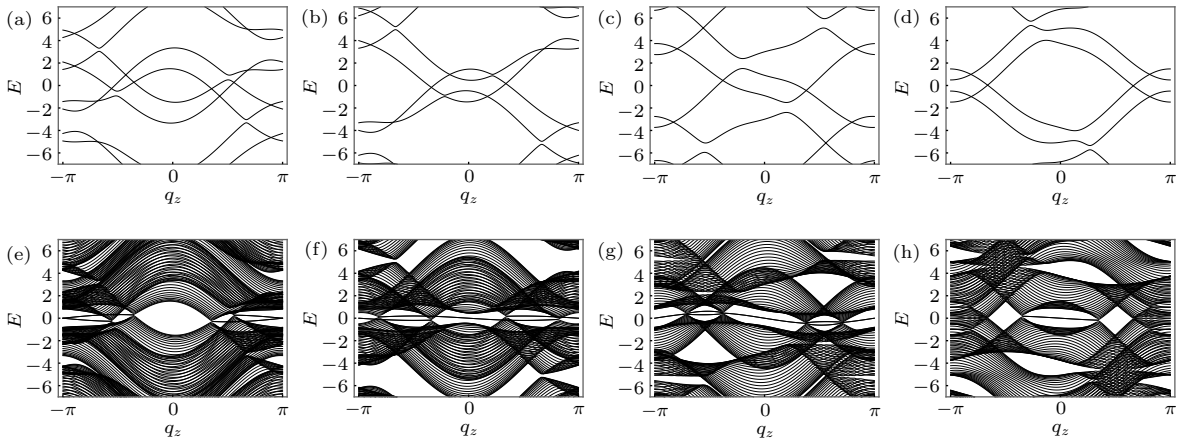



**Fig. A1.** Periodic and open boundary (along $y$-direction, $y = 30$) BdG Hamiltonian band structures. $M_0 = -8.5$, $M_1 = -3$, $M_2 = 3$, $q_x = 0$, $q_y = 0$, $\mu = 1$, $u = 1$ $\delta_{2,4,5,6} = 0$: (a), (e) $\delta_1 = 1$, $\delta_3 = 3$, (b), (f) $\delta_1 = 1$, $\delta_3 = 5$, (c), (g) $\delta_1 = 5$, $\delta_3 = 2$, (d), (h) $\delta_1 = 5$, $\delta_3 = 5$.

## Acknowledgment

Project supported by the National Natural Science Foundation of China (Grant Nos. 12174067 and 11804223).

## References

[1] Wan X, Turner A M, Vishwanath A and Savrasov S Y 2011 *Phys. Rev. B* **83** 205101
[2] Xu G, Weng H M, Wang Z J, *et al*. 2011 *Phys. Rev. Lett.* **107** 186806
[3] Weng H M, Fang C, Fang Z, *et al*. 2015 *Phys. Rev. X* **5** 011029

[4] Huang S M, Xu S Y, Belopolski I, *et al*. 2015 *Nat. Commun.* **6** 7373
[5] Lv B Q, Weng H M, Fu B B, *et al*. 2015 *Phys. Rev. X* **5** 031013
[6] Lv B Q, Xu N, Weng H M, *et al*. 2015 *Nat. Phys.* **11** 724
[7] Xu S Y, Belopolski I, Alidoust N, *et al*. 2015 *Science* **349** 613
[8] Hatsugai Y 1993 *Phys. Rev. Lett.* **71** 3697
[9] Wang Z, Sun Y, Chen X Q, *et al*. 2012 *Phys. Rev. B* **85** 195320
[10] Burkov A A, Hook M D and Balents L 2011 *Phys. Rev. B* **84** 235126
[11] Weng H M, Liang Y, Xu Q, *et al*. 2015 *Phys. Rev. B* **92** 045108
[12] Bradlyn B, Cano J, Wang Z J, *et al*. 2016 *Science* **353** 558
[13] Weng H M, Fang C, Fang Z, *et al*. 2016 *Phys. Rev. B* **93** 241202
[14] Li F Y, Li Y D, Kim Y B, *et al*. 2016 *Nat. Commun.* **7** 12691
[15] Prodan E and Prodan C 2009 *Phys. Rev. Lett.* **103** 248101
[16] Zhang L F, Ren J, Wang J S and Li B W 2010 *Phys. Rev. Lett.* **105** 225901
[17] He H, Qiu C, Ye L, *et al*. 2018 *Nature* **560** 61
[18] Khanikaev A B, Hossein M S, Tse W K, *et al*. 2013 *Nat. Mater.* **12** 233
[19] Chen W J, Jiang S J, Chen X D, *et al*. 2014 *Nat. Commun.* **5** 5782
[20] Ding K, Ma G C, Xiao M, *et al*. 2016 *Phys. Rev. X* **6** 021007
[21] Kitaev A 2003 *Ann. Phys. (NY)* **303** 2
[22] Kitaev A 2001 *Phys. Usp.* **44** 131
[23] Lian B, Sun X Q, Vaezi A, *et al*. 2018 *Proc. Natl. Acad. Sci. USA* **115** 10938
[24] Zhan Y M, Chen Y G, Chen B, *et al*. 2022 *New J. Phys.* **24** 043009
[25] Majorana E 1937 *Il Nuovo Cimento* **14** 171
[26] Fu L and Kane C L 2008 *Phys. Rev. Lett.* **100** 096407
[27] Wray L A, Xu S Y, Xia Y, *et al*. 2010 *Nat. Phys.* **6** 855
[28] Sato M 2006 *Phys. Rev. B* **73** 214502
[29] Yang S Y A, Pan H and Zhang F 2014 *Phys. Rev. Lett.* **113** 046401
[30] Sato M and Fujimoto S 2010 *Phys. Rev. Lett.* **105** 217001
[31] Zhang P, Yaji K, Hashimoto T, *et al*. 2018 *Science* **360** 182
[32] Zhang P, Wang Z J, Wu X X, *et al.* 2019 *Nat. Phys.* **15** 41
[33] Wang D F, Kong L Y, Fan P, *et al*. 2018 *Science* **362** 333
[34] Kamihara Y, Watanabe T, Hirano M, *et al*. 2008 *J. Am. Chem. Soc.* **130** 3296
[35] Bernevig B A, Hughes T L and Zhang S C 2019 *Science* **314** 1757
[36] Zhang H J, Liu C X, Qi X L, *et al*. 2009 *Nat. Phys.* **5** 438
[37] Zhang R X, Cole W S and Das Sarma S 2019 *Phys. Rev. Lett.* **122** 187001
[38] Wang Z J, Zhang P, Xu G, *et al.* 2015 *Phys. Rev. B* **92** 115119
[39] Nakosai S, Tanaka Y and Nagaosa N 2012 *Phys. Rev. Lett.* **108** 147003
[40] Zhang R X and Das Sarma S 2021 *Phys. Rev. Lett.* **126** 137001
[41] Fu L and Berg E 2010 *Phys. Rev. Lett.* **105** 097001
[42] Xu Y M, Huang Y B, Cui X Y, *et al*. 2011 *Nat. Phys.* **7** 198
[43] Ueno Y, Yamakage A, Tanaka Y, *et al*. 2013 *Phys. Rev. Lett.* **111** 087002
[44] Shiozaki K and Sato M 2014 *Phys. Rev. B* **90** 165114
[45] Sato M and Fujimoto S 2009 *Phys. Rev. B* **79** 094504
[46] Sedlmayr N, Kaladzhyan V, Dutreix C, *et al*. 2017 *Phys. Rev. B* **96** 184516
[47] Setiawan F, William S Cole, Jay D S, *et al*. 2017 *Phys. Rev. B* **95** 020501
[48] Schnyder A P, Brydon P M R, Manske D, *et al*. 2010 *Phys. Rev. B* **82** 184508
[49] Goll G 2006 *Physica B* **383** 71
[50] Altland A and Zirnbauer M R 1997 *Phys. Rev. B* **55** 1142